The Astrophysical Journal, 607:959–969, 2004 June 1

A COMPREHENSIVE STUDY OF THE X-RAY BURSTS FROM THE MAGNETAR CANDIDATE 1E 2259+586

Fotis P. Gavriil,[1] Victoria M. Kaspi,[1,2,3] and Peter M. Woods[4,5]
Received 2003 October 29; accepted 2004 February 12

ABSTRACT

We present a statistical analysis of the X-ray bursts observed from the 2002 June 18 outburst of the anomalous X-ray pulsar (AXP) 1E 2259+586, observed with the Proportional Counter Array (PCA) aboard the *Rossi X-Ray Timing Explorer*. We show that the properties of these bursts are similar to those of soft gamma repeaters (SGRs). We find the following similarities: the burst durations follow a lognormal distribution that peaks at 99 ms, the differential burst fluence distribution is well described by a power law of index -1.7, the burst fluences are positively correlated with the burst durations, the distribution of waiting times is well described by a log normal distribution of mean 47 s, and the bursts are generally asymmetric, with shorter rise than fall times. However, we find several quantitative differences between the AXP and SGR bursts. Specifically, the AXP bursts we observed exhibit a wider range of durations, the correlation between burst fluence and duration is flatter than for SGRs, the observed AXP bursts are on average less energetic than observed SGR bursts, and the more energetic AXP bursts have the hardest spectra—the opposite of what is seen for SGRs. Unlike the case of SGRs, we find a correlation of burst phase with pulsed intensity. We conclude that the bursts are sufficiently similar that AXPs and SGRs can be considered united as a source class, yet there are some interesting differences that may help determine what physically differentiates the two closely related manifestations of neutron stars.

Subject headings: pulsars: general — pulsars: individual (1E 2259+586) — X-rays: bursts — X-rays: general

1. INTRODUCTION

Soft gamma repeaters (SGRs) are an exotic class of Galactic sources that are now commonly accepted as being magnetars—isolated, young neutron stars that are powered by the decay of an ultrahigh magnetic field. The evidence for high surface fields ($\sim 10^{14}$–10^{15} G) comes from several independent lines of reasoning (Duncan & Thompson 1992; Paczyński 1992; Thompson & Duncan 1995, 1996). These include the high dipolar magnetic fields implied by the spin properties of SGRs seen in quiescence, under the assumption of magnetic dipole braking (Kouveliotou et al. 1998, 1999); the requirement of a magnetar-strength field to confine the energy released in the tails of hyper-Eddington outbursts seen from two SGRs (Mazets et al. 1979; Hurley et al. 1999); the requirement of a high field to allow the decay rate necessary to power the burst and persistent emission (Thompson & Duncan 1996; Goldreich & Reisenegger 1992); and the magnetic suppression of the Thomson cross section, which allows hyper-Eddington bursts to be observed (Paczyński 1992). For reviews of SGRs, see Kouveliotou (1999), Hurley (2000), and Thompson (2001).

Anomalous X-ray pulsars (AXPs), another exotic class of Galactic neutron stars, have also been suggested to be magnetars (Thompson & Duncan 1996). This is because of their anomalously bright X-ray emission, which can be explained by neither conventional binary accretion models nor rotation power (Mereghetti & Stella 1995). In addition, their spin parameters, as for SGRs, imply large magnetic fields under standard assumptions of magnetic braking. They also have X-ray spectra similar to, although on average softer than, those of SGRs in quiescence. However, unlike SGRs, in the more than 20 yr since the discovery of the first AXP (Fahlman & Gregory 1981), none was seen to exhibit SGR-like bursts. For this reason, alternative models involving unconventional accretion scenarios have been proposed to explain AXP emission (van Paradijs et al. 1995; Chatterjee et al. 2000; Alpar 2001). See Israel et al. (2002) and Mereghetti et al. (2002) for reviews of AXPs.

The magnetar model for AXPs was recently given a boost when SGR-like bursts were detected from two AXPs. Gavriil et al. (2002) reported on the discovery of two X-ray bursts in observations obtained in the direction of the AXP 1E 1048.1−5937. The temporal and spectral properties of those bursts were similar only to those seen only in SGRs. However, the AXP could not be definitely identified as the burster. On 2002 June 18, a major outburst was detected unambiguously from the AXP 1E 2259+586, involving over 80 bursts, as well as significant spectral and timing changes in the persistent emission (Kaspi et al. 2003). Those bursts demonstrated that AXPs are capable of exhibiting behavior observed, until now, uniquely in SGRs, therefore implying a clear connection between the two source classes. Such a connection was predicted only by the magnetar model (Thompson & Duncan 1996). However, the physical difference between the source classes is as yet unclear; Gavriil et al. (2002) and Kaspi et al. (2003) suggest that AXPs have higher surface magnetic fields than do SGRs, in spite of the evidence to the contrary from their spin-down properties.

In this paper, we consider the statistical properties of the 1E 2259+586 bursts in detail, in order to compare them quantitatively with SGR bursts, both to confirm that they have properties sufficiently similar that the two phenomena can definitely be unified and to look for subtle differences that may

[1] Department of Physics, Rutherford Physics Building, McGill University, 3600 University Street, Montreal, QC H3A 2T8, Canada.
[2] Department of Physics and Center for Space Research, Massachusetts Institute of Technology, Cambridge, MA 02139.
[3] Canada Research Chair, Steacie Fellow, CIAR Fellow.
[4] Space Science Research Center, National Space Science and Technology Center, Huntsville, AL 35805.
[5] Universities Space Research Association.

offer clues regarding the physical distinction between the two classes. Statistical studies of magnetar bursts (e.g., Göğüş et al. 1999, 2000, 2001) have the potential to yield important information regarding the burst energy injection and radiation mechanisms. Correlations between different burst properties, whether temporal or spectral, can be powerful model discriminators. Burst statistical properties can be compared with other physical phenomena in order to assist in identifying their underlying cause; for example, they have been used to argue for important similarities between SGR bursts and earthquakes (Cheng et al. 1996).

In this paper we present a comprehensive analysis of the properties of the bursts seen in the 2002 June 18 outburst of 1E 2259+586. We present a study of the detailed outburst and postoutburst properties of the persistent and pulsed emission of 1E 2259+586 in a companion paper (Woods et al. 2004).

2. OBSERVATIONS AND ANALYSIS

The results presented here were obtained using the Proportional Counter Array (PCA; Jahoda et al. 1996) aboard the *Rossi X-Ray Timing Explorer* (*RXTE*). The PCA consists of an array of five collimated xenon/methane multianode proportional counter units (PCUs) operating in the 2–60 keV range, with a total effective area of approximately 6500 cm^2 and a field of view (FOV) of $\sim 1^\circ$ FWHM. We use *RXTE* to monitor all five known AXPs on a regular basis as part of a long-term monitoring campaign (see Gavriil & Kaspi 2002 and references therein). On 2002 June 18, during one of our regular monitoring observations (*RXTE* observation identification 70094-01-03-00), which commenced at UT 15:39:18, the AXP 1E 2259+586 exhibited an SGR-like outburst (see Fig. 1; Kaspi et al. 2003). The bursting behavior was detected by online *RXTE* monitors during the observation and is clearly visible in the PCA "Standard 1" data. The observation spanned three orbits and had a total on-source integration time of 10.7 ks. Although some PCUs turned on or off during our observation, there were exactly three PCUs operational at all times. In addition to the standard data modes, data were collected in the Good Xenon with Propane mode, which records the arrival time (with 1 μs resolution) and energy (with 256 channel resolution) of every unrejected xenon event, as well as all the propane layer events. Processing of these data was done with software that operated directly on the raw telemetry data. Photon arrival times were adjusted to the solar system barycenter using a source position of R.A. $23^{\rm h}01^{\rm m}08^{\rm s}.295$, decl. $+58^\circ52'44''.45$ (J2000.0; Patel et al. 2001) and the JPL DE-200 planetary ephemeris. Note that following the outburst, Target of Opportunity observations of the source were initiated the next day and continued at different intervals over the subsequent weeks; however, no more bursts were seen.

2.1. *The Burst Identification Algorithm*

To study the bursts quantitatively, we made use of the Good Xenon with Propane data. Time series were created separately for each PCU using all xenon layers. Light curves of various time bin widths (1/1024, 1/256, 1/64, 1/32, and 1/16 s) were created to allow sensitivity to bursts on a range of timescales. The FTOOLs *xtefilt* and *maketime* were used to determine the intervals over which each PCU was off. We further restricted the data set by including only events in the energy range 2–20 keV. We used this energy range, which is larger than that used to study the quiescent pulsations

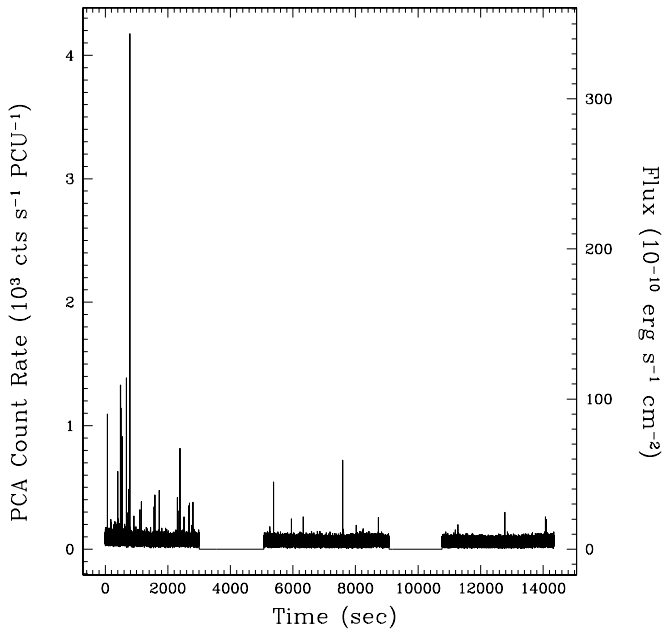

FIG. 1.—The 2–60 keV *RXTE* PCA light curve for 1E 2259+586 on 2002 June 18, at 62.5 ms resolution. The gaps are Earth occultations.

(Gavriil & Kaspi 2002; Woods et al. 2004), because of the much harder spectra of the bursts relative to the quiescent emission.

The following procedure was performed separately for each PCU, in order to identify bursts. First, for each data set, the number of counts in the ith time bin was compared to a local mean, μ_i. The local mean was calculated over a $\sim$28 s (four pulse periods) stretch of data centered around the time bin being evaluated. A window of $\sim$7 s (one pulse cycle) was also administered so that counts directly from, and immediately around, the point under investigation would not contribute to the local mean. During the outburst there was an increase in the pulsed flux (Kaspi et al. 2003; Woods et al. 2004), such that coherent pulsations were visible in our binned light curves. Because of this, for example, the apparent significance of bursts falling near a pulse peak would be artificially enhanced. To compensate for this effect, we first modeled the counts per time bin due to pulsations as

$$p_i = A(\phi_i, t_i)Ce^{-t_i/\tau}, \tag{1}$$

where $A(\phi, t)$ is the normalized amplitude of the pulsations as a function of pulse phase ϕ and time t. The parameters C and τ are from an exponential fit to the pulsed flux evolution. We then calculated an adjusted local mean in the following way:

$$\lambda_i = \mu_i + p_i - \sum_j p_j, \tag{2}$$

where the index j spans the windowed stretch of data used to calculate the local mean. For the number of counts in a time bin (n_i) greater than the adjusted local mean (λ_i), the probability of those counts occurring by random chance is given by

$$P_i = \frac{\lambda_i^{n_i} e^{-\lambda_i}}{n_i!}. \tag{3}$$

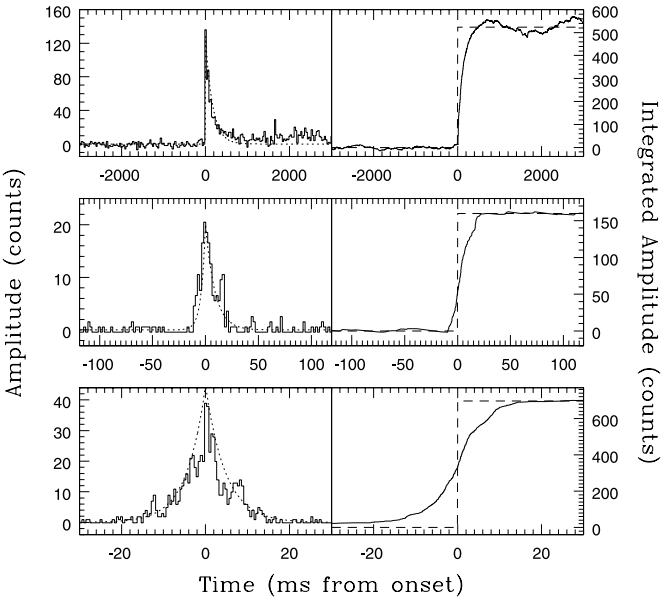

FIG. 2.—Three different examples of bursts seen in the 2002 June 18 outburst of 1E 2259+586. *Left*: Sample background-subtracted light curves in the energy range 2–60 keV with 1/32 s (*top*), 1/512 s (*middle*), and 1/2048 s (*bottom*) time resolution. The dotted line shows the model fitted to the data in order to measure burst rise and fall times (see § 3.1.4 for details). *Right*: Cumulative background-subtracted counts for each burst. The vertical dashed line shows the location of the burst peak. The horizontal dashed line shows the level used in determining the burst fluence. See § 3.1.2 for details.

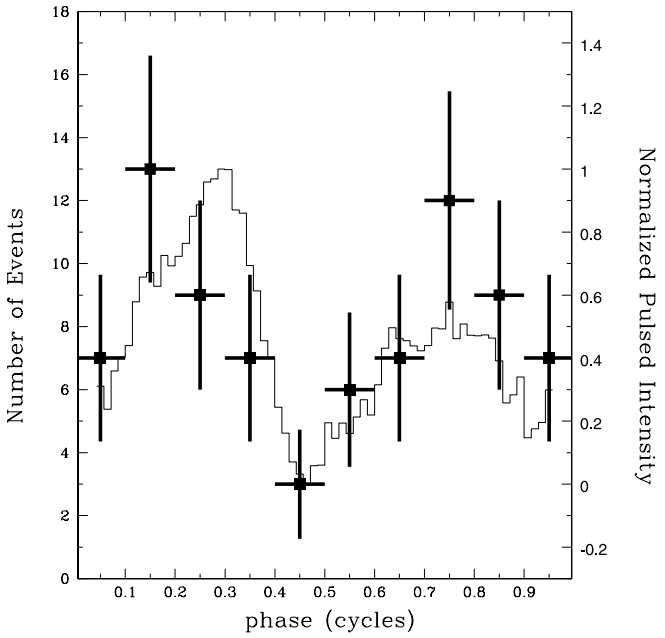

FIG. 3.—Distribution of the pulse phases of 1E 2259+586 that correspond to the times of the burst peaks (*squares*). The curve represents the folded 2–60 keV light curve of the 2002 June 18 observation with the bursts omitted.

As the probability P_i for each PCU is independent, we calculated the total probability ($P_{\rm tot}$) of observing a burst simultaneously with all operational PCUs as

$$P_{i,\rm tot} = \prod_{k=0}^{4} P_{i,k}, \tag{4}$$

and k corresponds to the PCU under consideration. If a particular PCU was inoperable, we set $P_{i,k} = 1$. Events that registered a value of $P_{i,\rm tot} \leq 0.01/N$, where N is the total number of time bins searched, were flagged as bursts and were subject to further investigation.

The significance of the number of counts in a time bin can be underestimated if there are one or more bursts in the interval used as the local mean. For this reason, once a burst was identified it was removed from the light curve, and the burst-identifying procedure was repeated until there were no additional bursts returned.

3. RESULTS

3.1. *Burst Statistics*

Our burst-searching algorithm returned 80 significant bursts from the 2002 June 18 observation—this is the total number of unique bursts identified on all timescales we searched. The number of bursts identified depended on the time resolution used: 26%, 55%, 76%, 83%, and 74% of all identified bursts were flagged at 1/1024, 1/256, 1/64, 1/32, and 1/16 s time resolution, respectively. The bursts were single-peaked and had durations $\lesssim$1 s. A small handful ($\sim$12) were bright and had clear fast-rise, exponential-decay morphology. In four instances we could not analyze bursts independently because one would fall on the long tail of another. A variety of burst morphologies is shown in Figure 2. Some bursts ($\sim$5%) were approximately symmetric; a few ($\sim$3%) fell faster than they rose, while most fell slower than they rose (see § 3.1.4).

3.1.1. *Burst Event Times and Phase*

The time of each burst was initially defined, using binned light curves, to be the midpoint of the bin having the most counts. To increase the precision of the burst time we refined this value, using the event data that comprised this time bin, to be the midpoint of the times of the events having the smallest temporal separation. We also calculated the occurrence in pulse phase for each burst, using the time of the burst peak and the rotational ephemeris given by Kaspi et al. (2003). Comparing the burst phase distribution to the pulse profile of 1E 2259+586 at the time of the outburst reveals a correlation (Fig. 3). To quantify it, we binned the pulse intensity with the same number of phase bins as the burst phase distribution. Least-squares fitting to a straight line yields reduced $\chi^2 = 0.6$. Although, when comparing our burst phase distribution to the mean number of bursts per phase bin, we find reduced $\chi^2 = 1.5$, the fact that most of the bursts tend to occur when the pulsed intensity is high is very suggestive. We note that the two bursts seen from the AXP 1E 1048.1−5937 (Gavriil et al. 2002) were also coincident with the pulse peak, which strengthens the argument that 1E 1048.1−5937 was the source of those bursts. We do not find any other significant correlation between burst phase and any another burst property discussed below.

3.1.2. *Burst Durations and Fluence*

The T_{90} duration is the time between when 5% and 95% of the total background-subtracted burst counts have been accumulated (e.g., Göğüş et al. 2001). The background count rate was determined by averaging a hand-selected, burst-free region before and after the burst. This typically consisted of two intervals of 1 s before and after the burst in question. The integrated background-subtracted counts were then fitted to a step function plus a linear term using least-squares fitting. The height of the step function corresponds to the total burst

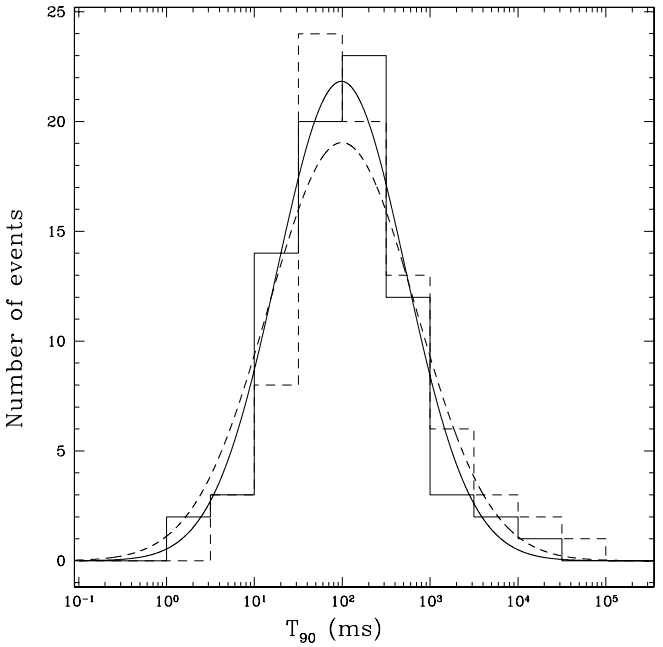

FIG. 4.—Distribution of T_{90} durations for the bursts observed from 1E 2259+586. The solid histogram shows the observed binned distribution (see § 3.1.2), while the dashed histogram shows the corrected distribution (see § 3.1.5). The solid curve represents the best-fit lognormal model for the observed data, as determined by maximum likelihood testing. The dashed curve represents the best-fit lognormal model for the corrected data. This fit has mean 99.31 ms and standard deviation of a factor of 6.9.

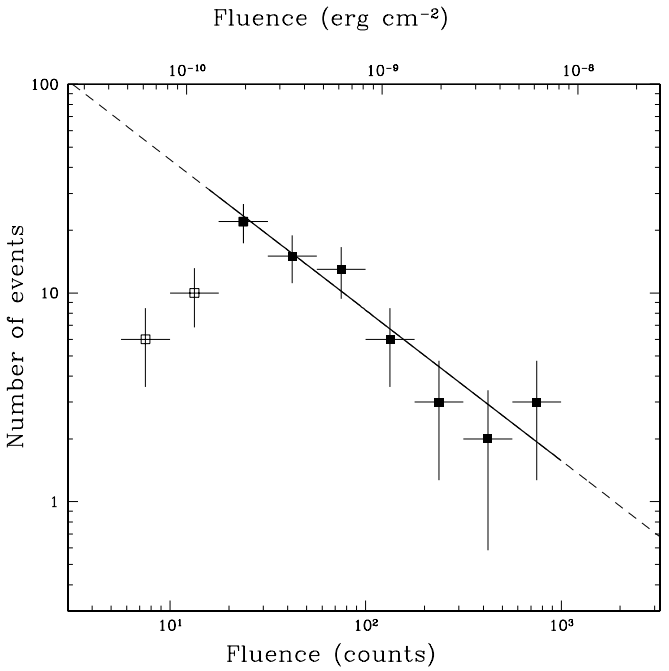

FIG. 5.—Distribution of the 2–60 keV fluence F for each burst observed from 1E 2259+586. Filled squares represent average values of fluence in equispaced logarithmic bins for which our observations had full sensitivity. The open squares represent values that suffered from reduced sensitivity. The best-fit line was determined using the filled squares only and is shown as a solid line; the dashed lines are its extrapolation. The slope of this line is -0.7 ± 0.1, which corresponds to $dN/dF \propto F^{-1.7}$.

fluence F (in counts), and the slope of the line corresponds to any background counts that were improperly subtracted.

SGR T_{90} distributions follow a lognormal distribution, defined as

$$P(T_{90},\, \mu,\, \hat{\sigma}) = \frac{1}{\log\hat{\sigma}\sqrt{2\pi}}\, \exp\left[-\frac{1}{2}\left(\frac{\log T_{90} - \log\mu}{\log\hat{\sigma}}\right)^2\right], \tag{5}$$

whose mean and standard deviation vary with source (e.g., Göğüş et al. 2001). At first, we fitted the measured values of T_{90} for the 1E 2259+586 bursts with this model and found it to characterize the distribution well. In equation (5), the parameters $\log\mu$ and $\log\hat{\sigma}$ correspond to the mean and standard deviation of the $\log T_{90}$ values. The mean of the T_{90} values is given by μ, and the range for one standard deviation corresponds to $(\mu\hat{\sigma}^{-1},\, \mu\hat{\sigma})$. The best-fit μ and $\hat{\sigma}$ were determined by maximum likelihood testing. The latter allowed us to extract model parameters that are independent of the arbitrarily chosen histogram bin widths. Specifically, the best-fit parameters were those that maximize the statistic

$$\mathcal{M} = \sum_{i=1}^{N} \log P\big(T_{90,\,i},\, \mu,\, \hat{\sigma}\big), \tag{6}$$

where N is the number of bursts. Figure 4 shows the distribution and best-fit lognormal model for the measured values. We found that our T_{90} distribution has a mean $\mu = 97.9$ ms, with a range of 18.2–527.2 ms for one standard deviation. Note, however, that for low–signal-to-noise ratio bursts, T_{90} can be substantially underestimated. We describe how we corrected for this problem and obtained slightly modified best-fit lognormal parameters in § 3.1.5.

The fluences, measured as described above, were then grouped in equispaced logarithmic bins. The distribution of burst fluences is displayed in Figure 5. The low-end fluences are underrepresented because of sensitivity drop-off. Excluding the points having fluence of $\lesssim$20 PCA counts, the distribution is well modeled by a simple power law. Using least-squares fitting, we find a best-fit power-law index of -0.7 ± 0.1, which corresponds to a differential spectrum $dN/dF \propto F^{-1.7\pm0.1}$. From the plot, it is clear that the fluences span approximately 2 orders of magnitude. For our calibration of the fluences in cgs units, see § 3.2.4.

Göğüş et al. (2001) also find a clear correlation between burst durations and total burst fluence. In Figure 6, we plot fluence versus T_{90}. A correlation can clearly be seen. To quantify it, we grouped the T_{90} values in equispaced logarithmic bins and determined group-averaged fluences for each bin. Least-squares fitting to a simple power-law model yields $F \propto T_{90}^{+0.54\pm0.08}$, with reduced $\chi^2 = 1.0$.

3.1.3. *Burst Peak Fluxes*

Burst peak fluxes were determined from the event data using the following algorithm. A boxcar integrator of width 62.5 ms was translated through the event data. The procedure began and ended when the center of the boxcar was at half a boxcar width before and after the time of the burst peak (as determined in § 3.1.1). At each boxcar step, a flux measurement was made by integrating the number of events and dividing by the boxcar width. The burst peak flux was assigned the largest such flux measurement. We then grouped our peak fluxes in equispaced logarithmic bins. The distribution of peak fluxes is shown in Figure 7.

Our burst-identifying algorithm is less sensitive to bursts of smaller peak flux. To compensate for this effect, we ran the

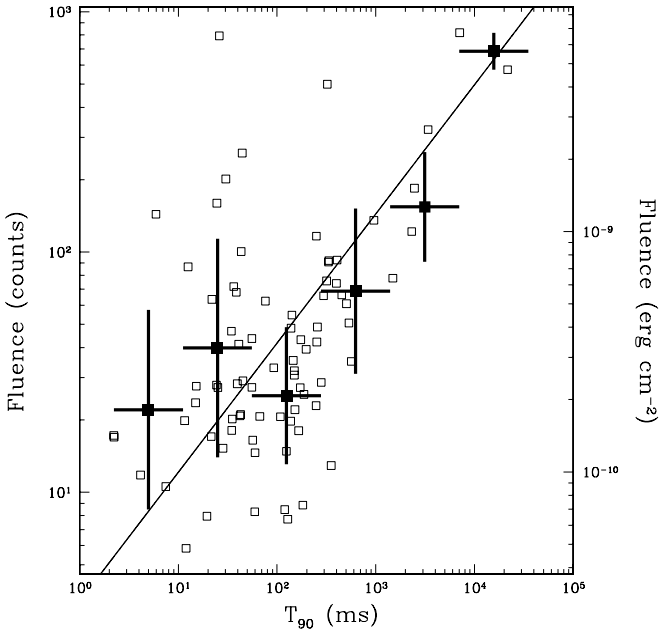

FIG. 6.—Burst 2–60 keV fluence vs. T_{90}. The open squares represent individual bursts. The filled squares represent binned averages. The line represents the best-fit power law for the binned averages. The slope of the line is $+0.54 \pm 0.08$.

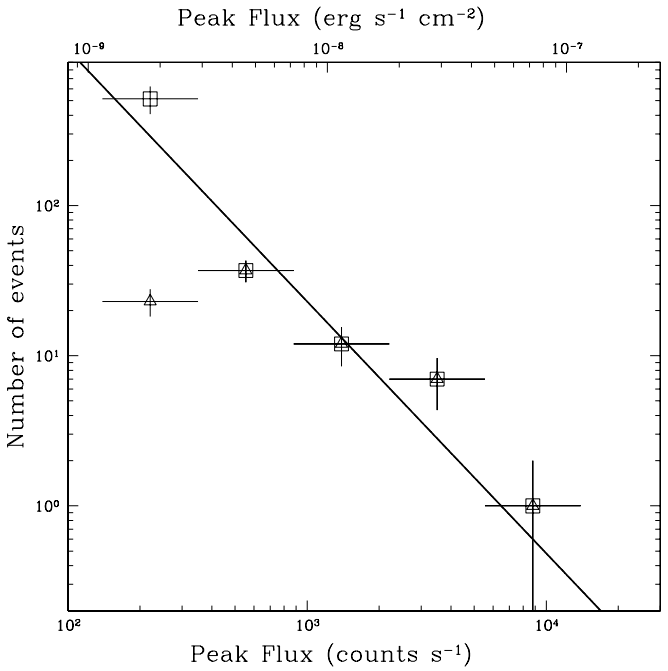

FIG. 7.—Distribution of burst peak flux for 62.5 ms time binning. The triangles represent observed averages in equispaced logarithmic bins. Our sensitivity is significantly reduced at low peak fluxes. The corrected values, determined using simulations described in § 3.1.3 are shown by open squares. The corrected flux bins were fitted with a power law, shown by a line. The slope is -1.42 ± 0.13.

following simulation. We took a hand-selected, 1 ks long, burst-free region from our observed 1E 2259+586 light curve binned with 62.5 ms resolution. We then injected a simulated burst having peak flux f_p at a random position in the light curve. We modeled the burst by a top-hat function of width $\Delta t = 62.5$ ms (one time bin) and height $f_p \Delta t$. We then ran our burst-identifying algorithm as described in § 2.1. We repeated this procedure for N_i iterations and determined N_s, the number of successful burst identifications for that simulated peak flux. We repeated the procedure for various peak fluxes and determined the probability of detecting a burst, $P = N_s/N_i$, as a function of peak flux f_p. We found that P could be well modeled by the following analytic function:

$$P(f_p) = \frac{1}{2}\left[1 + \tanh\left(\frac{f_p - f_0}{k}\right)\right], \tag{7}$$

with $f_0 = 309.84$ counts s^{-1} and $k = 58.21$ counts s^{-1}. We then used this function to correct our peak flux distribution (see Fig. 7, *squares*). Using least-squares fitting, we found that the corrected distribution is well modeled by a simple power law with index -1.42 ± 0.13. For our calibration of these peak fluxes in cgs units, see § 3.2.4.

3.1.4. *Burst Rise and Fall Times*

Burst rise and fall times were obtained from the event data by maximizing the likelihood of the assumed probability distribution,

$$P(t) = \begin{cases} A\left[C_p e^{(t-t_p)/t_r} + B\right] & t \le t_p \\ A\left[C_p e^{-(t-t_p)/t_f} + B\right] & t > t_p \end{cases}, \tag{8}$$

where B represents the background count rate, C_p represents the background-subtracted count rate at the time of the burst peak t_p, and t_r and t_f represent the burst rise and fall times, respectively. The parameter A is a normalizing factor ensuring unit probability over the interval of interest. This model characterized the bursts well—see the left-hand panels of Figure 2 (*dotted lines*) for examples. Burst rise and fall time distributions are displayed in Figure 8, with best-fit lognormal models determined via maximum likelihood testing. For the rise time distribution, we find a mean of 2.43 ms and a range of 0.51–11.51 ms for one standard deviation, with reduced $\chi^2 = 1.3$. For the fall time distribution, we find mean 13.21 ms a range of 3.52–49.55 ms for one standard deviation, and a reduced $\chi^2 = 0.2$. In order to better quantify burst morphologies, we also show the ratio of burst rise times to fall times (t_r/t_f; Fig. 8, *top*). On average, bursts rise faster than they fall; however, this is not universally true. Again fitting a lognormal distribution, we find mean 0.18 and a range of 0.03–1.08 for one standard deviation, with reduced $\chi^2 = 3.7$. The latter fit is poor because the distribution is clearly skewed toward shorter rise times. The asymmetry of the typical burst can also be seen in Figure 9, where the distribution of t_r/T_{90} is plotted.

3.1.5. *Corrected T_{90} Values*

Göğüş et al. (2001) showed that in the low–signal-to-noise ratio regime, the value of T_{90} can be underestimated. To account for this, a model light curve was generated for each burst, having the form of equation (8). Peak flux, rise time, and fall time were fixed at the values measured for that particular burst. The simulated light curve was then integrated, and the model duration ($T_{90,m}$) was measured by the same procedure outlined in § 3.1.2. We then repeated the procedure, with noise added to the simulated light curve. The noise was drawn from a Poissonian distribution having a mean equal to the measured background rate of the burst under investigation. We repeated the procedure for 200 realizations of noise. For

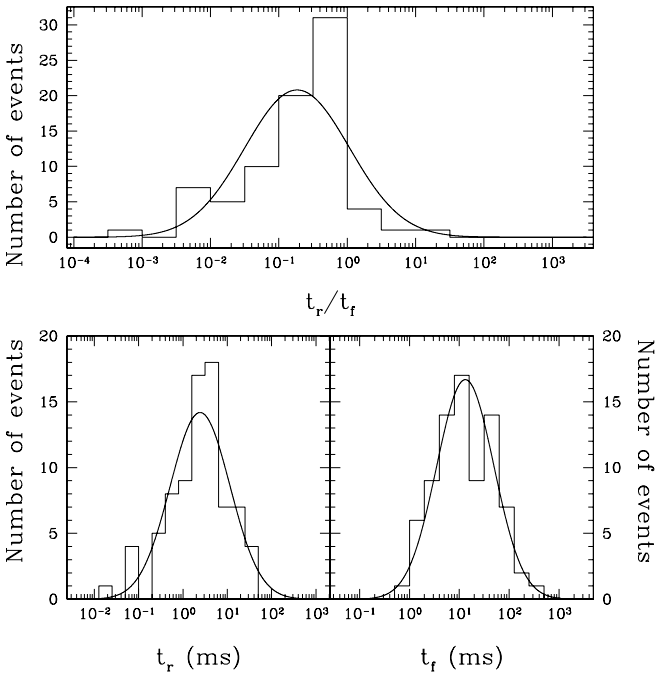

FIG. 8.—*Bottom*: Distribution of burst rise (t_r; *left*) and fall (t_f; *right*) times (see § 3.1.4). *Top*: Distribution of t_r/t_f. In all cases, the solid line represents the best-fit lognormal model, as determined by maximum likelihood testing.

each iteration (i) we measured the duration ($T_{90,i}$). The simulated durations ($T_{90,i}$) were normally distributed, and the mean of this distribution, ($T_{90,s}$), allowed us to calculate a correction factor $\mathcal{FD} \equiv 1 - T_{90,m}/T_{90,s}$. The corrected T_{90} distribution is shown in Figure 4. The best-fit mean is 99.31 ms, with a range of 14.4–683.9 ms for one standard deviation.

3.1.6. *Burst Waiting Times*

SGR waiting times (ΔT), defined as the temporal separations of adjacent bursts, are found to follow lognormal distributions (Göğüş et al. 1999, 2000). We measured the waiting time for the 1E 2259+586 events, excluding those interrupted by Earth occultations. Figure 10 displays our ΔT distribution with the best-fit lognormal model as determined by maximum likelihood testing. The best-fit parameters are a mean of 46.7 s and a range of 10.5–208.4 s for one standard deviation, with reduced $\chi^2 = 0.6$. We find no correlation between the burst energy or duration and either the waiting time until the next burst or the elapsed time since the previous burst.

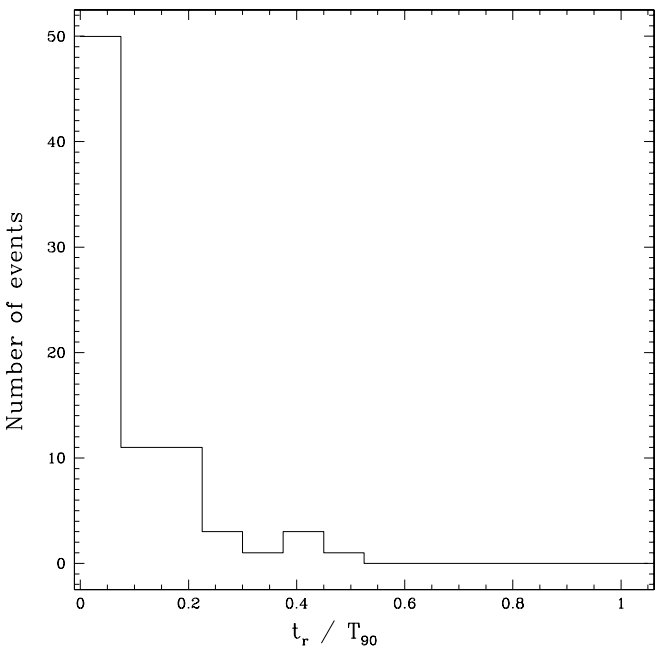

FIG. 9.—Distribution of the ratio of burst rise time t_r to duration T_{90}.

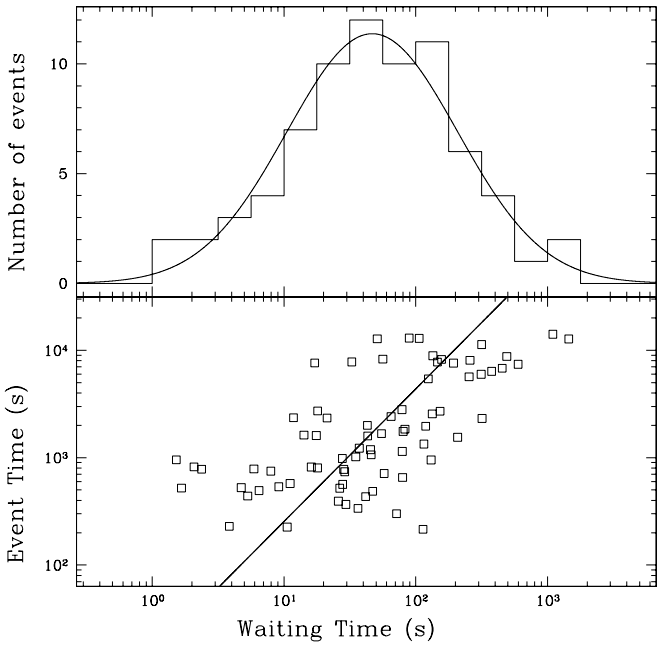

FIG. 10.—*Top*: Distribution of the waiting time between successive bursts. The solid curve represents the best-fit lognormal model, as determined by maximum likelihood testing. The mean is 46.8 s, with a standard deviation of a factor of 4.4. *Bottom*: Waiting time as a function of event time. The line represents the best-fit power-law model. The gaps in the event times are Earth occultations.

Note, however, that the burst rate clearly decreased during the observation (see Fig. 1). This is made clear by the bottom panel of Figure 10, which shows a correlation between the waiting time (ΔT) and the burst peak time (t_p). We fit this correlation to a power-law model using least-squares fitting, which reveals that $\Delta T = 0.11 t_p^{0.81}$. This correlation implies that the mean of our waiting time distribution depends on the time at which we started observing the outburst. We find no correlation between the burst energy or duration and when the bursts occur.

3.2. *Burst Spectroscopy*

3.2.1. *Individual Burst Spectra*

Spectra for each burst were extracted with the 256 spectral bins over the PCA range grouped by a factor of 4, in order to increase the signal-to-noise ratio per spectral bin. The same background intervals selected in measuring T_{90} were used in the spectral analysis (see § 3.1.2). In all spectral analyses, energies below 2 keV and above 60 keV were ignored, leaving on average 33 spectral channels for fitting. The regrouped spectra, along with their background estimators, were used as input to the X-ray spectral fitting software package XSPEC.[6] Response matrices were created using the FTOOLs *xtefilt* and

[6] See http://xspec.gsfc.nasa.gov.

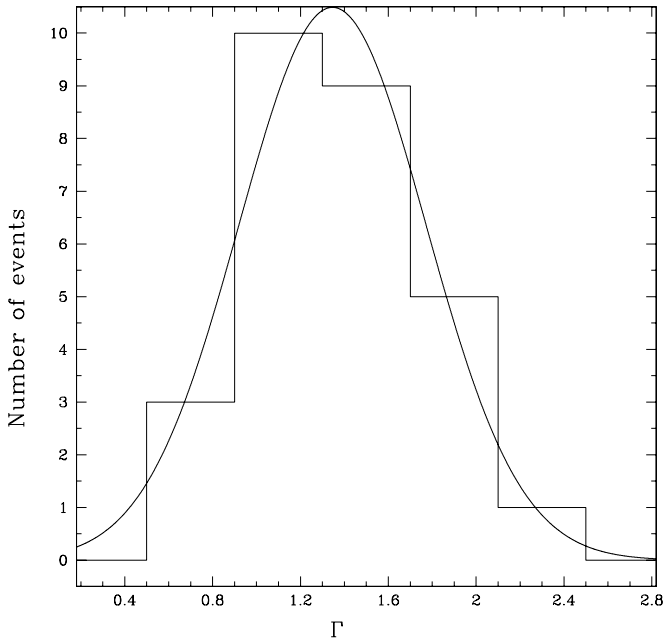

FIG. 11.—Distribution of spectral indices (Γ) for the 28 most fluent bursts. See § 3.2.1 for details. The curve is the best-fit Gaussian model. This fit has mean 1.35 and standard deviation 0.43.

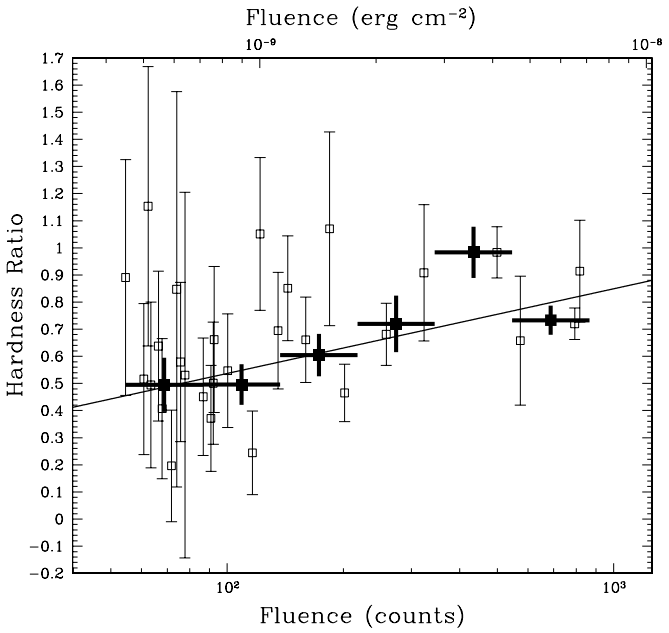

FIG. 12.—Hardness ratio (H) vs. fluence (F). Hardness ratio is defined as the ratio of the number of PCA counts in the 10–60 keV band to that in the 2–10 keV band. The open squares represent hardness ratio measurements for individual bursts. The filled squares represent weighted averages of hardness ratios for bursts in equispaced logarithmic fluence bins. The line represents the best-fit logarithmic function for the weighted averages, $H = 0.31 \log F - 0.09$.

pcarsp. We fitted the 28 most fluent bursts with a photoelectrically absorbed power law of index Γ, holding only $N_{\rm H}$ fixed at 0.93×10^{22} cm^{-2} (the value found by Patel et al. 2001). The distribution of spectral indices is shown in Figure 11. We find a mean spectral index of $\Gamma = 1.35$, with standard deviation 0.43.

3.2.2. *Hardness Ratios*

Göğüş et al. (2001) noted that SGR bursts tend to soften with increasing burst energy. We studied the hardness ratio–fluence relationship by extracting spectra and creating response matrices separately for each burst. The hardness ratio was defined as the ratio of the counts in the 10–60 keV band to those in the 2–10 keV band, as in Göğüş et al. (2001). Also following Göğüş et al. (2001), we divided the bursts into equispaced logarithmic fluence bins and calculated a weighted average hardness ratio for each bin. Figure 12 shows the weighted mean hardness ratios as a function of fluence. A clear positive correlation is seen. We repeated the procedure for different definitions of hardness ratio and found similar correlations. We further confirmed this trend by considering the 28 most fluent bursts for which spectral indexes Γ could be reliably and precisely constrained. All had Γ well below the mean value.

3.2.3. *Absence of Spectral Lines and the Average Burst Spectrum*

Possible spectral features have been reported in a burst from the AXP 1E 1048.1−5937 (Gavriil et al. 2002) and from bursts from two SGRs (Strohmayer & Ibrahim 2000; Ibrahim et al. 2002, 2003). In no spectrum of any burst for 1E 2259+586 did we detect a significant feature. In order to amplify any low-level spectral feature common to all bursts, we combined individual burst spectra to create a grand average spectrum. We summed the burst and background spectra described in § 3.2.1, using the FTOOL *sumpha*. Response matrices were scaled and added using the FTOOL *addpha*. Energies below 2 keV and above 60 keV were ignored, and spectral bins were grouped by a factor of 2, leaving 65 spectral channels for fitting. In order to search for features in the residuals, we fitted the combined spectrum to a simple, photoelectrically absorbed power law. The fit had reduced $\chi^2 = 1.3$ for 63 degrees of freedom. The residuals showed no evidence of significant spectral features.

3.2.4. *Calibrating Fluence and Flux*

Determining peak flux and total fluence distributions in cgs units requires spectral fitting. However, most bursts were too faint to allow spectral parameters to be determined with interesting precision. The problem was worse for the peak fluxes, since even the brighter bursts generally had too few counts to meaningfully constrain the spectrum. Therefore, we devised an alternate way of converting between PCA counts and cgs units. We took the spectra of the 40 most luminous bursts extracted over their T_{90} duration and fitted them with photoelectrically absorbed power laws. However, this time, for consistency, we held Γ fixed at the mean of our spectral index distribution. We multiplied the flux (in units of ergs s^{-1} cm^{-2}) in the 2–60 keV range returned by the fit by its respective T_{90} duration to obtain a fluence in units of ergs cm^{-2}. We then considered the 2–60 keV fluence in counts, as determined in § 3.1.2, as a function of the fluence in cgs units and determined the proportionality constant between the two, using least-squares fitting. This constant was found to be 8.226×10^{-12} ergs cm^{-2} counts^{-1}. In § 3.2.2, we found significant spectral evolution as a function of fluence. A change of 1 σ in spectral index Γ corresponds to a change by a factor of ∼1.5 in our calibration constant. The same procedure and constant apply for the peak fluxes. The cgs energy scales are shown at the top of Figures 5 and 7. The fluences in the 2–60 keV band range from $\sim 5 \times 10^{-11}$ to $\sim 7 \times 10^{-9}$ ergs cm^{-2}. These imply burst energies in the range $\sim 5 \times 10^{34}$ to

$\sim 7 \times 10^{36}$ ergs, assuming isotropic emission and a distance of 3 kpc to the source (Kothes et al. 2002). The sum total of all burst fluences is 5.6×10^{-8} ergs cm^{-2}, corresponding to energy of 6.0×10^{37} ergs (2–60 keV). Peak fluxes in a 61.25 ms time bin range from $\sim 1 \times 10^{-9}$ to $\sim 1 \times 10^{-7}$ ergs cm^{-2} s^{-1}, implying peak luminosities in the range $\sim 1 \times 10^{36}$ to $\sim 1 \times 10^{38}$ ergs s^{-1}. On shorter timescales, we find five bursts with peak fluxes that are super-Eddington. The peak fluxes in a 1/2048 s time bin for these bursts range from $\sim 2 \times 10^{38}$ to $\sim 8 \times 10^{38}$ ergs s^{-1}.

4. DISCUSSION

Here we compare the various measured quantities for the AXP and SGR bursts. Note that our comparisons focus primarily on PCA observations of SGRs 1806−20 and 1900+14, for consistency of spectral and temporal response. Göğüş et al. (2001) observed SGR 1900+14 using *RXTE* between 1996 November 5 and 18. Their observations had a total integration time of 224.1 ks, and a total of 837 bursts were identified using the full PCA bandpass. In their statistical analysis, they concentrated on 679 bursts clustered together during two very burst-active epochs. Similarly, Göğüş et al. (2001) observed SGR 1806−20, using *RXTE* between 1998 June 2 and December 21. These observations had a total integration time of 136.8 ks, and a total of 290 bursts were identified using the full PCA bandpass. In their analysis for this source, they focused on 268 bursts clustered together during a very burst-active period of the source between 1998 August 29 and September 2.

4.1. *Similarities between AXP and SGR bursts*

As we describe below, many of the properties of the bursts seen from 1E 2259+586 during its 2002 June 18 outburst are very similar to those seen in SGRs. Specifically,

1. the burst T_{90} durations follow a lognormal distribution that peaks at 99.31 ms;
2. the differential burst fluence spectrum is well described by a power law of index -1.7, similar to those seen in SGRs (and earthquakes and solar flares);
3. burst fluences are positively correlated with burst durations;
4. the distribution of waiting times is well described by a lognormal distribution, with a mean of 46.7 s;
5. the burst morphologies are generally asymmetric, with rise times usually shorter than burst durations.

The mean T_{90} value of 99.31 ms (see § 3.1.5 and Fig. 4) is very similar to those seen for SGRs 1806−20 and 1900+14: 161.8 and 93.9 ms, respectively. Göğüş et al. (2001) suggested that the difference between these values for the two SGRs is a result of a difference in an intrinsic physical property of the sources, such as the strength of magnetic field or the size of the active region. Given the generally softer persistent emission spectra of AXPs compared to SGRs, as well as the less frequent outbursts of the AXPs, it is reasonable to suspect that the two source classes also differ by some physical property; age (Kouveliotou et al. 1998; Gaensler et al. 2001), magnetic field (Gavriil et al. 2002; Kaspi et al. 2003), and progenitor mass (Gaensler 2004) have been proposed. The similarity of the burst durations of all three sources implies, however, that the physical property resulting in different mean burst durations must be different from the one that results in different average spectra and outburst frequency.

The distribution of burst fluences for 1E 2259+586 is remarkably similar to those seen in SGRs. For the 1E 2259+586 bursts, we find a fluence distribution $dN/dF \propto F^{-1.7 \pm 0.1}$ (Fig. 5). Göğüş et al. (2000) showed that for the PCA, the fluence distribution for SGR 1806−20 is well described by a power law of index -1.43 ± 0.06, while at higher burst energies, the index steepens to -1.7. For SGR 1900+14, Göğüş et al. (1999) found an index of $-1.66^{+0.13}_{-0.12}$ extending over the full range of burst fluences. The good agreement of the fluence distribution indices shows that for a given outburst intensity (i.e., the normalization of the fluence distribution), the average burst energy is the same for 1E 2259+586 as it is for these two SGRs. The difference between the SGR outbursts that are routinely detected by IPN detectors and this outburst from 1E 2259+586, which was not detected by the IPN, is that the SGR outbursts have shown higher outburst intensities. Since we know that the SGRs spend most of their time in quiescence, when the fluence distribution normalization is zero (or near zero), the dynamic range of the outburst intensities in SGRs is larger than has been observed thus far in 1E 2259+586. This difference in range is intrinsically even larger when one considers that 1E 2259+586 is believed to be significantly closer (3 kpc) than either of these two SGRs (∼15 kpc; Vrba et al. 2000; Corbel et al. 1997).

Cheng et al. (1996) noted the similarity of the fluence distribution index for SGR 1806−20 with that determined empirically for earthquakes (Gutenberg & Richter 1956a, 1956b, 1965) and also for the distribution of earthquake energies found in computer simulations (Katz 1986). However, solar flares also show a size distribution, with exponents ranging from 1.53 to 1.73 (Crosby et al. 1993; Lu et al. 1993). Magnetars are not clearly physically analogous to either system; in magnetars, magnetic stresses are thought to result in stellar crust cracking, which is not the case for earthquakes. The bursts could be magnetic reconnections, as in solar flares (Lyutikov 2002); however, in the solar case there is no solid crust to yield, unlike in magnetars. The similarity of the distributions could be explained as a result of the phenomenon of self-organized criticality (Bak et al. 1988), in which a system is dynamically attracted (i.e., self-organized) to a critical, spatially self-similar state that is just barely stable to perturbations. In other words, the burst statistics alone do not constrain their physical origin.

It is not possible to compare peak flux distributions, as none are published for SGRs. For the AXP, the range of 2–60 keV peak flux for the 62.5 ms timescale spans a factor of ∼100, ranging from $\sim 1 \times 10^{-9}$ to $\sim 1 \times 10^{-7}$ ergs cm^{-2} s^{-1}, which, for a distance of 3 kpc, corresponds to luminosities of $\sim 1 \times 10^{36}$ to $\sim 1 \times 10^{38}$ ergs s^{-1}. At timescales as short as 1/2048 s, we find peak fluxes as high as $\sim 8 \times 10^{38}$ ergs s^{-1}. Thus, five bursts are above the Eddington limit on this timescale.

The waiting time distributions of the AXP and SGRs are very similar. All are well described by lognormal distributions. This is similar to what is seen in other self-organized critical systems, such as earthquakes (Nishenko & Buland 1987). For 1E 2259+586, we find a mean waiting time between bursts of 47 s and a range of 10–208 s. Göğüş et al. (1999) found ∼49 s for SGR 1900+14, and Göğüş et al. (2000) found ∼97 s for SGR 1806−20, with a range between ∼0.1 and 1000 s for both, very similar to our results. The absence of correlation between waiting time and burst fluence for the AXP is similar to that seen for SGRs (Göğüş et al. 1999, 2000), although Göğüş et al. (1999) report an

anticorrelation between time since the previous burst and burst energy. We do not see this for the AXP, nor do Göğüş et al. (2000) observe it for SGR 1806−20.

The morphologies of the AXP and SGR bursts are similar, with most being asymmetric, with faster rises than decays. Rise and fall time distributions for the SGRs have not been published, so we can compare neither those parameters directly nor the ratio of the two. Göğüş et al. (2001) showed the distribution of the ratio t_r/T_{90} for SGRs 1806−20 and 1900+14; the same plot for 1E 2259+586 looks similar (Fig. 9). We note that two bursts had T_{90} durations greater than the spin period of the source. These bursts have profiles similar to those of others, and we do not see any evidence of breaks in their profiles due to the occultation by the star.

4.2. *Differences between AXP and SGR Bursts*

As shown in § 4.1, many of the properties of the bursts seen from 1E 2259+586 during its 2002 June 18 outburst are very similar to those seen by Göğüş et al. (2001) in SGRs 1900+14 and 1806−20. However, there are some quantitative differences between the properties of the AXP and SGR bursts. The differences can be summarized as follows:

1. There is a significant correlation of burst phase with pulsed intensity, unlike in SGRs (see Palmer 1999, 2002; Lenters et al. 2003).
2. The AXP bursts have a wider range of burst duration (although this may be partly due to different analysis procedures).
3. The correlation of burst fluence with duration is flatter for AXPs than it is for SGRs (although when selection effects are considered, this correlation should really be seen as an upper envelope for AXPs and SGRs).
4. The fluences for the AXP bursts are generally smaller than those in observed SGR bursts.
5. In the AXPs, the more energetic bursts have the hardest spectra, whereas in the SGR, they have the softest.
6. Under reasonable assumptions, SGRs undergo outbursts much more frequently than do AXPs.

The standard deviation of the T_{90} distribution for the 1E 2259+586 bursts is much larger than that for the SGR bursts. For 1E 2259+586, the 1 σ range is from $\sim$14 to $\sim$684 ms, or 1.7 orders of magnitude. For SGRs 1806−20 and 1900+14, the durations span 0.68 and 0.70 orders of magnitude, respectively. The lower bound on the 1E 2259+586 distribution may be artificially lower because of the shorter timescales searched in this work, as compared to that of Göğüş et al. (2001), who searched for SGR bursts on the 0.125 s timescale. However, such a wide range of durations is seen even when faint bursts are omitted from the T_{90} distribution of 1E 2259+586. Göğüş et al. (2001) argued that if the "trapped fireball" model, which describes the giant SGR bursts well, also applies to the fainter bursts, then the narrowness of the T_{90} distribution, compared with the wide range of fluences, demands a planar fireball geometry. This is because the duration of the burst is limited by the rate of cooling through the radiative fireball surface layer. For 1E 2259+586, the T_{90} range is larger than the fluence range, indicating that if the fireball model applies, a planar fireball geometry is not supported.

As in SGRs, the fluences of the 1E 2259+586 bursts are significantly positively correlated with T_{90} (Fig. 6). However, there is one difference: for the AXP, the relationship is well described by a power law of index $+0.54 \pm 0.08$, while for SGRs 1806−20 and 1900+14, Göğüş et al. (2001) found $+1.05 \pm 0.16$ and $+0.91 \pm 0.07$, respectively. Thus, the power-law index for AXPs is half that seen in SGRs. It is important to recognize, however, that severe selection effects are at work here. Specifically, as discussed in § 3.1.2, we are less sensitive to low-fluence bursts. This is particularly true for bursts having long rise times, which will tend to have long T_{90} values. Thus, there are severe selection effects against finding bursts in the bottom right-hand portion of Figure 6, as there are in similar analyses for SGRs. Therefore, the above correlation should really be seen as an upper envelope to the phase space available to the burst. By contrast, our sensitivity to bursts that would sit in the upper left-hand corner of the plot is generally enhanced relative to the populated region, indicating that the absence of bursts in this part of phase space is genuine.

One striking difference between the AXP and SGR bursts is in the relationship between spectral hardness ratio and fluence. For SGR 1806−20, Göğüş et al. (2001) found that the more energetic bursts are spectrally softer, regardless of burst morphology. This was not seen for SGR 1900+14, however. Our analysis (see Fig. 12) shows the opposite behavior to that seen in SGR 1806−20, with the more energetic bursts having harder spectra. Göğüş et al. (2001) argued that the behavior seen for SGRs could be explained either by the emitting plasma being in local thermodynamic equilibrium, having radiative area decreasing for lower fluences, or by the spectral intensity of the radiation field being below that of a blackbody and hence the emitting plasma temperature T remaining in a narrow range, being higher at lower luminosities. Which of these two applies depends on the rate of energy injection into the magnetosphere; the latter applies only if the luminosity is less than $\sim 10^{42}(V^{1/3}/10)$ ergs s^{-1}, where V is the injection region, assuming a spherical geometry. Clearly, neither can apply for the AXP. Göğüş et al. (2001) imply that blackbody emission from a constant radius predicts the relationship between hardness and fluence that we find for the AXP. However, for the AXP, naively taking Figure 6 at face value, $F \propto T_{90}^{0.5}$. Hence, $L_a \propto F^{-1}$, so blackbody emission from a constant radius predicts $T \propto F^{-1/4}$, the opposite of what we have observed. We note further that the range of hardness ratios for the AXP bursts is slightly greater than it is for the SGRs. For 1E 2259+586, hardness ratios (for bursts having 10^2–10^3 counts) range from $\sim$0.54 to 0.85, while the range is $\sim$0.82–0.95 for SGR 1806−20 and $\sim$0.63–0.67 for SGR 1900+14 (Göğüş et al. 2001). It should be noted, however, that we identified bursts (see § 2.1) using a different energy range (2–20 keV) than Göğüş et al. (2001), who used the full bandpass of the PCA. This would make us more sensitive to softer bursts, which would affect the dynamic range of the hardness ratios we measured. Perhaps interestingly, for the SGRs, $F \propto T_{90}$, so the $L_a \equiv F/T_{90} \simeq$ constant, and for constant radiative area and blackbody emission, one expects $T \simeq$ constant, closer to what is observed for SGRs than for AXPs. Thus, although blackbody emission from a constant radius (not surprisingly) does not describe any of the data well, it does seem possible that the flatter dependence of fluence on T_{90}, the inverted dependence of hardness on fluence relative to the SGRs, and the greater range of hardness in the AXP bursts may all be related phenomena telling us something interesting about the physical distinction between these closely related sources.

We have stated that outbursts from AXPs similar to or larger than the one studied here are less frequent than are those from SGRs. Of course, given that we have observed only one AXP outburst and that this outburst was energetically smaller

and fainter than observed SGR outbursts, making a meaningful comparison of their outburst rate is very difficult. We can estimate the rate of AXP outbursts of the magnitude of the 2002 June 18 event as follows. We consider data from only our *RXTE* PCA monitoring program, as it provides a consistent, quasi-regularly sampled data set with a single instrument. The monitoring program for 1E 2259+586 has extended over nearly 7 yr, with only one such outburst detected; even though the bursting appears to have been relatively short-lived, the effects of a glitch of even much smaller size would easily have been detected throughout the data span. We make the admittedly speculative assumption that all such outbursts are accompanied by comparably sized glitches. A comparable glitch in the AXP 1RXS 1708−4009 was recently detected in 5.4 yr of monitoring without evidence of radiative outburst; however, the sparse observations could have missed one (Kaspi & Gavriil 2003; Dall'Osso et al. 2003). Two small bursts have been seen in 6.8 yr of timing of the AXP 1E 1048.1−5937 (Gavriil et al. 2002); all the measured properties of these two bursts fall within the range of burst properties found for 1E 2259+586. The timing behavior of 1E 1048.1−5937 suggests that many glitches could be occurring (Kaspi et al. 2001); however, no other evidence of radiative outbursts has been found. No activity of any kind, apart from apparently simple timing noise, has been seen in 6.5 yr of timing of 4U 0142+61 (Gavriil & Kaspi 2002) or in 4.3 yr of timing 1E 1841−045 (Gotthelf et al. 2002). If we omit 1E 1048.1−5937, whose timing behavior we do not fully understand, we can estimate a rough AXP outburst rate of one every 11 yr, assuming that the glitch in 1RXS 1708−4009 was indeed a similar outburst, or one every ∼22 yr, if not. SGRs, by contrast, burst much more frequently, reach higher intensities, and persist for longer periods of time. The monitoring of the SGRs with the *RXTE* PCA has not been as regular as that for the AXPs because of less optimal observing conditions for the SGRs (lower pulsed fractions and source flux, stronger timing noise, etc.); therefore, we cannot make a direct comparison of the outburst recurrence rate using the PCA data. We can, however, make a rough estimate of the recurrence rate, using results obtained with the Burst and Transient Source Experiment (BATSE) that flew aboard the *Compton Gamma-Ray Observatory*. The advantage of using BATSE to estimate the SGR outburst rate is its uniform and dense coverage in time due to its "all-sky" FOV. The disadvantage is that BATSE is much less sensitive to SGR bursts than is the PCA (e.g., Göğüş et al. 1999). Since SGR/AXP burst energies follow a steep power-law distribution, the outburst recurrence rate is a strong function of detector sensitivity. It follows that an outburst recurrence rate determined by BATSE will then be a lower limit to the rate for the more sensitive PCA. Moreover, the relative distances of AXPs and SGRs must be considered when determining intrinsic source rates for a given luminosity or total energy, as opposed to peak flux and fluence. With these factors in mind, we now estimate the SGR outburst recurrence rate at the BATSE sensitivity level. BATSE was in operation for 9.1 yr, from 1991 April through 2000 June. During that time, three of the four known SGRs entered outburst (Kouveliotou et al. 1993, 1994; Woods et al. 1999; Göğüş et al. 2001), some multiple times. Here, we define an outburst as a collection of bursts (i.e., more than two) in which the separation between consecutive bursts never exceeds one month. Using the results reported in Göğüş et al. (2001), the number of SGR outbursts detected during this time interval is 14. This yields an outburst rate for the SGRs of once every ∼2.6 yr. Recall that this is a lower limit to the rate at the PCA sensitivity level. Thus, the SGRs clearly undergo outbursts more frequently than do AXPs.

5. CONCLUSIONS

The bursts we have observed for 1E 2259+586 are clearly similar to those seen uniquely in SGRs. As concluded by Gavriil et al. (2002) and Kaspi et al. (2003), AXPs and SGRs clearly share a common nature, as has been predicted by the magnetar model. In this paper, we have done a quantitative analysis of the 1E 2259+586 bursts seen on 2002 June 18 and compared our results with those obtained for the two best-studied SGRs, 1806−20 and 1900+14. The bursts seen in the 2002 June 18 outburst of 1E 2259+586 are qualitatively similar to those seen in SGRs and in many ways quantitatively similar. However, there are some interesting quantitative differences between the properties of the AXP and SGR bursts. These may help shed light on the physical difference(s) between these classes. Given the rarity of AXP bursts, coupled with the unique information that detection of such bursts provides, observing more outbursts is obviously desirable. Continued monitoring is thus clearly warranted, and *RXTE*, with its large area and flexible scheduling, is the obvious instrument of choice.

We are grateful to C. Kouveliotou, M. Lyutikov, S. Ransom, M. S. E. Roberts, D. Smith, and C. Thompson for useful discussions. This work was supported in part by NSERC, NATEQ, CIAR, and NASA. This research has made use of data obtained through the High Energy Astrophysics Science Archive Research Center Online Service, provided by the NASA Goddard Space Flight Center.

REFERENCES

Alpar, M. A. 2001, ApJ, 554, 1245
Bak, P., Tang, C., & Wiesenfeld, K. 1988, Phys. Rev. A, 38, 364
Chatterjee, P., Hernquist, L., & Narayan, R. 2000, ApJ, 534, 373
Cheng, B., Epstein, R. I., Guyer, R. A., & Young, A. C. 1996, Nature, 382, 518
Corbel, S., Wallyn, P., Dame, T. M., Durouchoux, P., Mahoney, W. A., Vilhu, O., & Grindlay, J. E. 1997, ApJ, 478, 624
Crosby, N. B., Aschwanden, M. J., & Dennis, B. R. 1993, Sol. Phys., 143, 275
Dall'Osso, S., Israel, G. L., Stella, L., Possenti, A., & Perozzi, E. 2003, ApJ, 599, 485
Duncan, R. C., & Thompson, C. 1992, ApJ, 392, L9
Fahlman, G. G., & Gregory, P. C. 1981, Nature, 293, 202
Gaensler, B. M. 2004, Adv. Space. Res., 33, 645
Gaensler, B. M., Slane, P. O., Gotthelf, E. V., & Vasisht, G. 2001, ApJ, 559, 963
Gavriil, F. P., & Kaspi, V. M. 2002, ApJ, 567, 1067
Gavriil, F. P., Kaspi, V. M., & Woods, P. M. 2002, Nature, 419, 142
Göğüş, E., Kouveliotou, C., Woods, P. M., Thompson, C., Duncan, R. C., & Briggs, M. S. 2001, ApJ, 558, 228
Göğüş, E., Woods, P. M., Kouveliotou, C., van Paradijs, J., Briggs, M. S., Duncan, R. C., & Thompson, C. 1999, ApJ, 526, L93
———. 2000, ApJ, 532, L121
Goldreich, P., & Reisenegger, A. 1992, ApJ, 395, 250
Gotthelf, E. V., Gavriil, F. P., Kaspi, V. M., Vasisht, G., & Chakrabarty, D. 2002, ApJ, 564, L31
Gutenberg, B., & Richter, C. F. 1956a, Bull. Seismological Soc. Am., 46, 105
———. 1956b, Ann. Geofis., 9, 1
———. 1965, Seismicity of the Earth and Associated Phenomena (2nd ed.; New York: Hafner)
Hurley, K. 2000, in AIP Conf. Proc. 510, The Fifth Compton Symp., ed. M. L. McConnell & J. M. Ryan (New York: AIP Press), 515

Hurley, K., et al. 1999, Nature, 397, 41
Ibrahim, A. I., Safi-Harb, S., Swank, J. H., Parke, W., Zane, S., & Turolla, R. 2002, ApJ, 574, L51
Ibrahim, A. I., Swank, J. H., & Parke, W. 2003, ApJ, 584, L17
Israel, G., Mereghetti, S., & Stella, L. 2002, Mem. Soc. Astron. Italiana, 73, 465
Jahoda, K., Swank, J. H., Giles, A. B., Stark, M. J., Strohmayer, T., Zhang, W., & Morgan, E. H. 1996, Proc. SPIE, 2808, 59
Kaspi, V. M., & Gavriil, F. P. 2003, ApJ, 596, L71
Kaspi, V. M., Gavriil, F. P., Chakrabarty, D., Lackey, J. R., & Muno, M. P. 2001, ApJ, 558, 253
Kaspi, V. M., Gavriil, F. P., Woods, P. M., Jensen, J. B., Roberts, M. S. E., & Chakrabarty, D. 2003, ApJ, 588, L93
Katz, J. I. 1986, J. Geophys. Res., 91, 10412
Kothes, R., Uyaniker, B., & Yar, A. 2002, ApJ, 576, 169
Kouveliotou, C. 1999, Proc. Natl. Acad. Sci., 96, 5351
Kouveliotou, C., et al. 1993, Nature, 362, 728
———. 1994, Nature, 368, 125
———. 1998, Nature, 393, 235
———. 1999, ApJ, 510, L115
Lenters, G., et al. 2003, ApJ, 587, 761
Lu, E. T., Hamilton, R. J., McTiernan, J. M., & Bromund, K. R. 1993, ApJ, 412, 841
Lyutikov, M. 2002, ApJ, 580, L65
Mazets, E. P., Golenetskii, S. V., Il'inskii, V. N., Apetkar', R. L., & Gur'yan, Yu. A. 1979, Nature, 282, 587
Mereghetti, S., Chiarlone, L., Israel, G. L., & Stella, L. 2002, in Neutron Stars, Pulsars and Supernova Remnants, ed. H. W. Becker & J. Trümper (MPE Rep. 278; Garching: MPE), 29
Mereghetti, S., & Stella, L. 1995, ApJ, 442, L17
Nishenko, S. P., & Buland, R. 1987, Bull. Seismological Soc. Am., 77, 1382
Paczyński, B. 1992, Acta Astron., 42, 145
Palmer, D. M. 1999, ApJ, 512, L113
———. 2002, Mem. Soc. Astron. Italiana, 73, 578
Patel, S. K., et al. 2001, ApJ, 563, L45
Strohmayer, T. E., & Ibrahim, A. I. 2000, ApJ, 537, L111
Thompson, C. 2002, Mem. Soc. Astron. Italiana, 73, 477
Thompson, C., & Duncan, R. C. 1995, MNRAS, 275, 255
———. 1996, ApJ, 473, 322
van Paradijs, J., Taam, R. E., & van den Heuvel, E. P. J. 1995, A&A, 299, L41
Vrba, F. J., Henden, A. A., Luginbuhl, C. B., Guetter, H. H., Hartmann, D. H., & Klose, S. 2000, ApJ, 533, L17
Woods, P. M., et al. 1999, ApJ, 524, L55
———. 2004, ApJ, 605, 378